

THIS REPORT HAS BEEN DELIMITED
AND CLEARED FOR PUBLIC RELEASE
UNDER DOD DIRECTIVE 5200.20 AND
NO RESTRICTIONS ARE IMPOSED UPON
ITS USE AND DISCLOSURE.

DISTRIBUTION STATEMENT A

APPROVED FOR PUBLIC RELEASE;
DISTRIBUTION UNLIMITED.

UNCLASSIFIED

AD 401 529

*Reproduced
by the*

DEFENSE DOCUMENTATION CENTER

FOR

SCIENTIFIC AND TECHNICAL INFORMATION

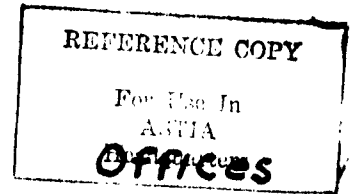
CAMERON STATION, ALEXANDRIA, VIRGINIA



UNCLASSIFIED

NOTICE: When government or other drawings, specifications or other data are used for any purpose other than in connection with a definitely related government procurement operation, the U. S. Government thereby incurs no responsibility, nor any obligation whatsoever; and the fact that the Government may have formulated, furnished, or in any way supplied the said drawings, specifications, or other data is not to be regarded by implication or otherwise as in any manner licensing the holder or any other person or corporation, or conveying any rights or permission to manufacture, use or sell any patented invention that may in any way be related thereto.

CATALOGED BY ASTIA
AS AD No. 401529



MICHIGAN STATE UNIVERSITY
PHYSICS DEPARTMENT
ULTRASONICS LABORATORY

401 529

Office of Naval Research
Contract Nonr-2587(01)
Project No. NR 385-425

OPTICAL METHODS FOR ABSOLUTE MEASUREMENT OF
SOUND PRESSURE IN LIQUIDS.

Technical Report No. 7.

E. A. Hiedemann
Main Investigator



March 1963

NO OTS

This Technical Report consists of papers prepared or published between July and December 1962 by the staff and graduate students supported by the Office of Naval Research, Acoustics Programs.

TABLE OF CONTENT.

- I. B. D. Cook, "New Procedure for Computing Finite-Amplitude Distortion". J. Acoust. Soc. Am., 34, 941 (1962).
- II. B. D. Cook, "Calculation of Finite-Amplitude Distortion", 4th Intern. Congr. Acoustics, paper J41 (1962).
- III. L. E. Hargrove, "Optical Effects of Ultrasonic Waves Producing Phase and Amplitude Modulation", J. Acoust. Soc. Am., 34, 1547 (1962).
- IV. W. G. Meyer, "On the Conversion of Longitudinal to Surface Waves in Solids", 4th Intern. Congr. Acoustics, paper P13 (1962).
- V. W. G. Meyer, "Reflection and Refraction of Mechanical Waves at Solid-Liquid Boundaries".
- VI. Distribution List.

New Procedure for Computing Finite-Amplitude Distortion

BILL D. COOK

Department of Physics, Michigan State University, East Lansing, Michigan

(Received November 21, 1961)

An iterative process is described for the calculation of the distortion of plane finite-amplitude sound waves in a dissipative, nondispersive medium. The method of calculation is a discrete-interval process of considering the distortion of the wave while propagating through a small distance, correcting for absorption within this distance, and then considering this new wave, etc. It is necessary to use a high-speed electronic computer to obtain the spectral composition of the wave. The iterative process allows calculations beyond the "discontinuity distance." The spatial change of the spectral composition is used for the calculation of "absorption coefficients" describing the energy loss from the total wave and from the fundamental component. These absorption coefficients, which are functions of distance from the source, are found to be remarkably different.

INTRODUCTION

IN recent years the problem of finite-amplitude sound waves has been approached through the solution of the nonlinear equation of motion. Although this approach has answered some of the questions concerning the propagation of finite-amplitude waves, the range of reliability of these theories, which are usually based on equations approximating the exact differential equation, is small. The reliability of this usually extends up to the neighborhood of the "discontinuity distance." However, from the phenomenological aspects of the problem, one can formulate a very simple model from which solutions at greater distances may be obtained. Presented here is such a model. While it necessitates the use of a high-speed electronic computer, it allows one to compute, by an iterative process, the spectral composition of the waves at *all* distances. It is not the purpose of this paper to correlate the results of previous theoretical and experimental investigations, but rather to show what may be obtained from a very simple model. The readers are referred to the papers of Keck and Beyer¹ and Zarembo and Krasil'nikov² for reviews of existing analyses using the differential equation.

A model approach was previously used by Fox and Wallace,³ who used a graphical analysis to determine the spectral composition and consequently determined an "absorption coefficient" for finite-amplitude waves.

Although the model here is based somewhat on the same assumptions as those of the Fox and Wallace theory, a more basic aspect of the absorption mechanism is introduced. A high-speed electronic computer is used to calculate the distortion. A parametric integration method similar to that given by Fubini-Ghiron⁴ is used. This integral method of Fubini-Ghiron has also been given by Hargrove⁵ and Keck and Beyer.¹

This model is based on two fundamental assumptions which describe the distortion and absorption mechanisms. These assumptions are the following:

- (1) The distortion mechanism can be described by a change in phase velocity directly proportional to the particle velocity.
- (2) The absorption mechanism can be described by assuming that the rate of the absorption of each harmonic is proportional to the amount of the harmonic present and to the square of the frequency of the harmonic.

These basic postulates are applied to a wave by first allowing the wave to distort while it propagates through a small interval, and then correcting for absorption. This wave of new shape is now allowed to distort and be absorbed. By assuming that no discontinuity of the wave shape is formed because of absorption, one may calculate by this continuing process the shape of the wave at all distances. Although the absorption and generation of the harmonics are treated independently

¹ W. Keck and R. T. Beyer, *Phys. Fluids* 3, 346-352 (1960).

² L. K. Zarembo and V. A. Krasil'nikov, *Soviet Phys.—Uspekhi* 2, 580-599 (1959).

³ F. E. Fox and W. A. Wallace, *J. Acoust. Soc. Am.* 26, 994-1006 (1954).

⁴ R. Fubini-Ghiron, *Alta Frequenz.* 4, 530 (1935).

⁵ L. E. Hargrove, *J. Acoust. Soc. Am.* 32, 511-512 (1960).

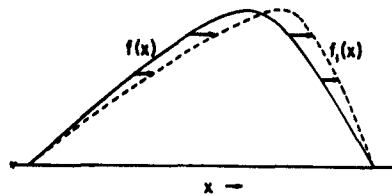


FIG. 1. Diagram showing the distortion process postulated for a finite-amplitude wave.

in each small interval, the end result contains the interaction between absorption and generation mechanisms.

Others^{6,7} have considered similar absorption mechanisms along with distortion; however, the effect of the absorption on the generation of the harmonics is neglected. The range of these theories which are based on the Fubini-Ghiron method does not exceed the discontinuity distance as given by the dissipationless theory.

The model presented here is not expected to be valid for extremely intense sound waves which may produce periodic shock fronts but rather for sound waves of moderate amplitudes traveling in a fairly absorbing medium. In particular, this model should be useful for the investigation of finite-amplitude waves of the megacycle frequencies in liquids. The calculations presented from this model are for a range of parameters which cover the practical experimental situations.

FORMULATION OF THE MODEL

In this paper we shall consider plane acoustic waves in a nonlinear, nondispersive medium. Following the usual notation we write an equation relating the instantaneous pressure p and density ρ as

$$p = p_0 + A \left(\frac{\rho - \rho_0}{\rho_0} \right) + \frac{B}{2} \left(\frac{\rho - \rho_0}{\rho_0} \right)^2. \quad (1)$$

The zero subscripts refer to the undisturbed medium. The terms A and B are constants for a given medium at a given temperature. Using the above equation of state, the phase velocity is

$$c = c_0 + [B/(2A) + 1]u, \quad (2)$$

accurate to the first order in u , where u is the particle velocity and c_0 is the velocity of sound with infinitesimal amplitude. It is assumed here that this linear change of phase velocity with particle velocity is the only mechanism which causes the wave to distort. Points on the wave having larger values of particle velocity tend to overtake points of lesser values. For a dissipationless medium, an initially sinusoidal waveform will become multiple valued at distances greater than a distance L

given by¹

$$L = c_0^2 \{ 2[B/(2A) + 1] f \pi U_1(0) \}^{-1}, \quad (3)$$

where f is the frequency of the wave and $U_1(0)$ is the maximum particle velocity of the initial wave. This distance L (known as the "discontinuity distance") shall become one of the important parameters in describing the results from this model approach.

The exact frequency dependence of the absorption coefficient for most media is unknown.⁸ Here we shall assume for simplicity that the rate of absorption is proportional to the square of the frequency of the wave; this is characteristic of a viscous, heat-conducting medium.

In the absorption of infinitesimal waves, the exponential decay which describes the "diffusive nature" of the absorption, occurs because the damping forces produced are proportional to the quantity being damped. Although for acoustic waves in a viscous, heat-conducting medium, the exponential decay arises from a higher-order differential equation, we shall assume that the "diffusive nature" can be described by a first-order differential equation, namely, the rate of absorption of a quantity is proportional to that quantity. However, in considering the "diffusive" absorption of waves, the exponential is a special case. It requires that the quantity being absorbed will remain at a constant value if the absorption mechanism vanishes. However, since the amplitudes of the harmonics are changing due to distortion while undergoing absorption, the diffusive absorption process must be considered for each harmonic according to its growth. The harmonics are treated independently, i.e., the absorption of a harmonic in a wave is the same as the absorption of an infinitesimal wave of that harmonic. Details of how the generation affects the rate of the absorption are given in the Appendix.

With these distortion and absorption mechanisms, it is relatively easy to calculate the spectral composition of a finite amplitude wave by an iterative process. In such a process, the results are expected to be more valid for smaller increments of interval. No analytical treatment will be given here for the estimate of size of these intervals in terms of the other parameters. It should be noted, however, that for small absorption parameters or greater amplitudes of the wave, the wave approaches more closely to the dissipationless case. For these conditions, it is reasonable to assume that intervals must be small.

DETAILS OF COMPUTATIONS

To calculate the effects of distortion, we shall now generalize the method outlined by Hargrove⁵ for the dissipationless case. Let a function $u = f(x)$ describe the particle velocity at a given time. The independent

¹ W. W. Lester, *J. Acoust. Soc. Am.* **33**, 1196 (1961).

² L. Adler, "A Study of the Distortion of Finite Amplitude Ultrasonic Waves in Liquids," M.S. thesis, Michigan State University, East Lansing, Michigan, 1961.

³ J. J. Markham, R. T. Beyer, and R. B. Lindsay, *Revs. Modern Phys.* **23**, 353-411 (1952).

variable is a reduced spatial coordinate which describes the function in the range $0 \leq x \leq 2\pi$. For simplicity we shall now restrict $f(x)$ to be an odd function. For arbitrary waveforms this restriction can be removed. During a small interval of time Δt , the whole waveform propagates a distance $c_0 \Delta t$. However, in addition to this velocity c_0 , each point of the wave described by the function u is assumed to propagate at a velocity proportional to the value of the function. The velocity of each point is given by Eq. (2). Figure 1 shows one half of an arbitrary waveform [described by $f(x)$] and the resultant waveform [described by $f_1(x)$] from such a distortion mechanism. The problem now is to calculate the function $f_1(x)$ provided that $f(x)$ and B/A are known.

As $f(x)$ is an odd function, $f_1(x)$ is necessarily an odd function. Thus both can be expanded in a Fourier sine series. Let

$$f(x) = \sum_{n=1}^{\infty} b_n \sin nx \quad (4)$$

and

$$f_1(x) = \sum_{n=1}^{\infty} b_{n,1} \sin nx. \quad (5)$$

If $f_1(x)$ is known, the expansion coefficients can be calculated from

$$b_{n,1} = \frac{2}{\pi} \int_0^{\pi} f_1(x) \sin nx dx. \quad (6)$$

Graphically, one may obtain $f_1(x)$ if $f(x)$ is known and thus obtain the coefficients $b_{n,1}$. By parametric integration, one may, in principle, analytically find these coefficients if $f(x)$ and B/A are known.

To evaluate Eq. (6) let

$$u = f[x(\theta)], \quad (7)$$

where

$$x(\theta) = \theta + kf(\theta). \quad (8)$$

The term $kf(\theta)$ describes the distortion mechanism as required by Eq. (2). The value of k is restricted to be sufficiently small, such that the waveform does not become multiple valued. Hargrove has shown that k represents the fractional distance to the discontinuity distance L of an initially sinusoidal wave. In other words, if in a dissipationless medium an initially sinusoidal wave propagates through a distance R , the spectral composition can be calculated using $k = R/L$. Substitution of Eqs. (7) and (8) into Eq. (6) gives

$$b_{n,1} = \frac{2}{\pi} \int_0^{\pi} \{f(\theta) \sin[n\theta + nkf(\theta)]\} \{1 + kf'(\theta)\} d\theta. \quad (9)$$

Thus if we know the description of the particle velocity at any given time, we can find the description of the particle velocity at a new time if we are considering only the distortion mechanism.

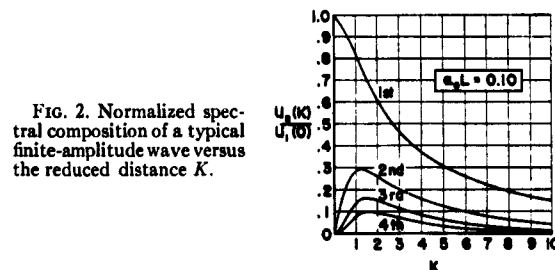


FIG. 2. Normalized spectral composition of a typical finite-amplitude wave versus the reduced distance K .

The procedure for introducing absorption is the following: assume a waveform (described by the coefficients $b_{n,i}$); choose a small increment of k ; calculate the spectral composition of a distorted wave by Eq. (9) (in terms of coefficients $b_{n,i+1}$); correct the coefficients (then described by $b_{n,i+1}$) for absorption; and repeat the above process using the previous results to describe the new wave. Each coefficient $b_{n,i+1}$ is corrected independently according to the assumption that the absorption throughout the small interval of k is proportional to the amount of the harmonic present at any given point in the interval. The frequency dependence of the absorption must be considered.

From the dissipationless theory,

$$b_n = (-1)^n (2/nk) J_n(nk). \quad (10)$$

It can be seen that $\Delta b_{n,i} (= b_{n,i+1} - b_{n,i})$ is approximately described by the first term of the power-series expression of Eq. (10) in the form $\Delta b_{n,i} = a_{n,i} k^{n-1}$ for small k . Assuming this power dependence on k , the absorption-corrected coefficients can be written as

$$b_{n,i+1} = b_{n,i} \exp(-\alpha_0 n^2 L k) + \Delta b_{n,i} A_{n-1}(\alpha_0 n^2 L k). \quad (11)$$

The first term of the right-hand side of Eq. (11) is the exponential decay if $\Delta b_{n,i} = 0$; α_0 is the absorption coefficient of a wave of the fundamental frequency and infinitesimal amplitude. The function $A_{n-1}(\alpha_0 n^2 L k)$ corrects for the absorption of the changing function $\Delta b_{n,i}$. This function A_{n-1} , which is described in the Appendix, is a power series for which the exponential power series is a special case. The n -squared dependence of the exponential and A_{n-1} is introduced by the assumption of the frequency squared dependence of the absorption. The product kL gives the actual distance that the wave propagates for the increment k .

For the calculations presented here the initial waveform is assumed to be sinusoidal with the unit amplitude ($b_{1,0} = 1$). The corresponding particle velocity and pressure may be determined through the parameter L . The results are expressed in terms of the product $\alpha_0 L$ and the reduced distance K . This distance K , which is the distance that the wave has propagated from the origin, is given by $K = mk$, where m is the number of intervals. When $K = 1$, the wave has propagated a distance equal to the discontinuity distance.

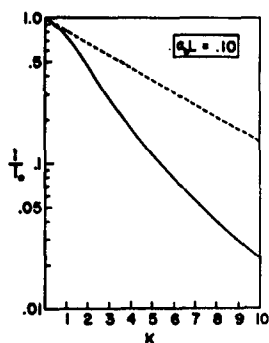


FIG. 3. Comparison of the normalized intensity (solid line) calculated from spectral curves of Fig. 2 and the exponential decay expected for a wave undergoing no finite-amplitude distortion.

The calculations were done by the Michigan State integral computer. To accurately retain the shape of the waveform, as many as 16 harmonics were computed for each interval. In the results presented here, the value of k never exceeds 0.05, one-twentieth of the discontinuity distance.

DISCUSSION OF RESULTS

Figure 2 shows the spectral composition of a wave from a typical calculation using this model. This composition is given in terms of the harmonic structure of the particle velocity. The amplitudes $U_n(K)$ of the harmonics are normalized to the particle velocity amplitude $U_1(0)$ of the initial sinusoidal wave. The value of $\alpha_0 L$ equals 0.10 for these calculations which extend to 10 times the discontinuity distance. For this cal-

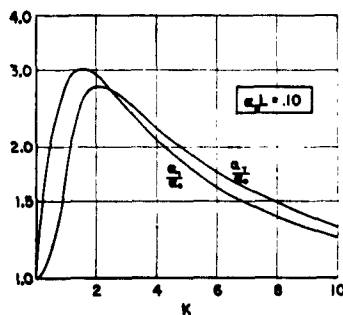


FIG. 4. Normalized absorption coefficients for the total wave α_T/α_0 and for the fundamental component α_1/α_0 for the values given in Figs. 2 and 3.

ulation, the amplitudes of higher harmonics peak in the region $1 < K < 2$.

Figure 3 shows the effect of the nonlinear propagation on the dissipation of the sound intensity calculated from the curves presented in Fig. 2. As is expected, there is a large difference between an exponential decay and the decay predicted by this model. The predicted greater total absorption is, of course, caused by the higher rate of absorption of the generated harmonics. To describe this higher rate of absorption, one may define a finite amplitude absorption coefficient¹ as

$$\alpha_T = -(1/2I)(dI/dx),$$

where I is the intensity of the sound wave. This coefficient α_T describes the rate at which the energy of the total wave is dissipated at any given distance. One may also define an absorption coefficient which describes the rate of loss of energy from the fundamental component alone as

$$\alpha_1 = -d(U_1^2)/2U_1^2 dx = -dU_1/U_1 dx.$$

Figure 4 shows these coefficients (normalized to α_0) for $\alpha_0 L = 0.10$. It is important to stress that the absorption coefficient for the fundamental frequency α_1 differs from the total absorption coefficient α_T for most values of K . It can, therefore, be concluded that the total

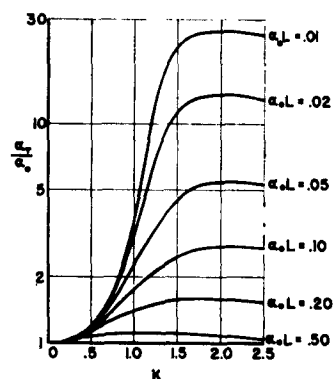


FIG. 5. Normalized total absorption coefficients for various values of $\alpha_0 L$.

absorption coefficient is not determined by experimental measurements of the fundamental component only. The difference between coefficients α_1 and α_T can be very large, especially at small distances; the energy of the fundamental is being lost by both distortion and absorption while the energy of the total wave is being lost only by absorption.

As to be expected, the values of α_T/α_0 and α_1/α_0 depend on the parameter $\alpha_0 L$. Figures 5 and 6 show the results for α_T/α_0 and α_1/α_0 , respectively, for various values of the parameter $\alpha_0 L$. For large values of $\alpha_0 L$ (larger than 0.50), which means either high absorption, small pressure, or small nonlinearity, the absorption

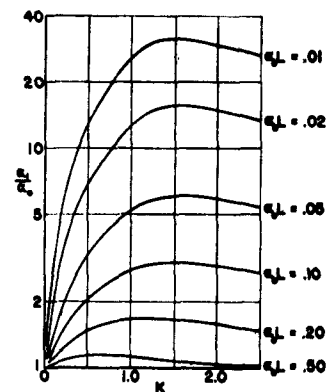


FIG. 6. Normalized fundamental absorption coefficient for various values of $\alpha_0 L$.

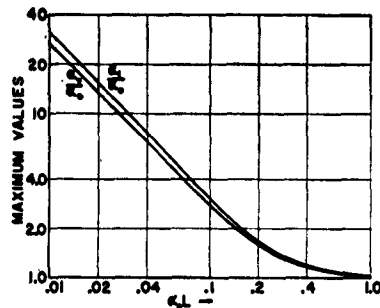


FIG. 7. The maximum values of the normalized absorption coefficients versus the parameter $\alpha_0 L$.

coefficients α_T and α_1 are nearly equal to α_0 . However, for small values of $\alpha_0 L$, these absorption coefficients become large compared to α_0 . Also at small values of K , the absorption coefficients, α_T and α_1 , differ greatly. For example, for $K=0.50$ and $\alpha_0 L=0.01$, the ratio α_1/α_T is approximately equal to 10.

The maximum values of α_T/α_0 and α_1/α_0 for values of $\alpha_0 L < 0.10$ occur in the neighborhood of $K=2.0$, and $K=1.5$, respectively. The dependence of the maximum values of α_T/α_0 and α_1/α_0 on $\alpha_0 L$ is shown in Fig. 7.

In Fig. 8 the fundamental component is shown for several values of $\alpha_0 L$. As $\alpha_0 L$ decreases, the values of $U_1(K)/U_1(0)$ are approaching upper limits. Of course,

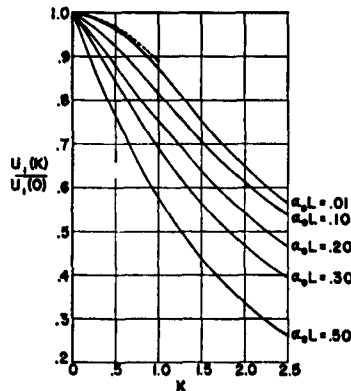


FIG. 8. Normalized fundamental component for various values of $\alpha_0 L$. Dashed line gives values of dissipationless theory.

for $K < 1$ the limiting values are those given by the dissipationless theory, not only for the fundamental, but also for the higher harmonics.

Figure 9 shows the effect of the parameter $\alpha_0 L$ on the second harmonic. For values of $\alpha_0 L < 0.20$, the maximum value of the second harmonic occurs at $K \approx 1.25$. For larger values of $\alpha_0 L$, these maxima are seen to occur at lower values of K . Similarly, the maximum values of the third and fourth harmonics are affected by the parameter $\alpha_0 L$ as shown in Figs. 10 and 11. As a consequence of the frequency squared dependence of the absorption, these higher harmonics

tend to become negligible even at moderate values of $\alpha_0 L$.

CONCLUSION

An iterative process is used to determine the spectral composition of plane finite-amplitude waves in a dissipative medium. From the spatial change of the amplitudes of the harmonic components, "absorption coefficients" describing the loss of the energy from the total wave and from the fundamental component are computed. The results are presented as families

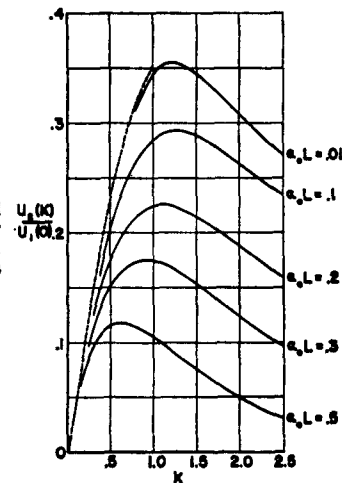


FIG. 9. Normalized second harmonic for various values of $\alpha_0 L$. Dashed line gives values of dissipationless theory.

of curves having the parameter $\alpha_0 L$. This parameter determines the experimental situation as α_0 , the absorption coefficient of the fundamental component of infinitesimal amplitude, and L , the "discontinuity distance," describes the absorption and distortion mechanisms.

ACKNOWLEDGMENTS

The author sincerely wishes to thank Dr. E. A. Hiedemann for his discussions and interest in this study.

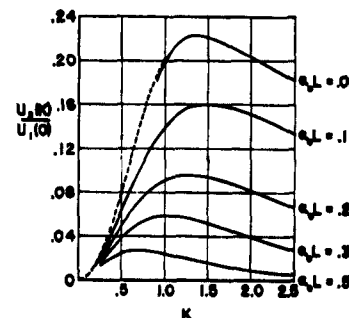


FIG. 10. Normalized third harmonic for various values of $\alpha_0 L$. Dashed line gives values of dissipationless theory.

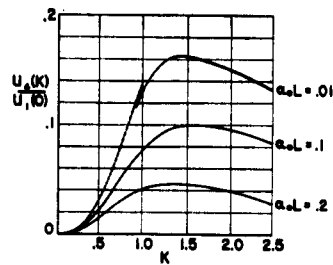


FIG. 11. Normalized fourth harmonic for various values of $\alpha_0 L$. Dashed line gives values of dissipationless theory.

The work was supported by the U. S. Army Research Office (Durham) and by the Office of Naval Research.

APPENDIX

By assuming the rate of loss of a quantity to be proportional to the quantity present at each instant, one expects a decay of the quantity according to an exponential law. However, this is true only if the quantity would remain constant if the loss mechanism were absent. We shall consider here the case where the quantity changes according to a power law in the interval if absorption were not present.

Let the dependence of the quantity y on the independent variable x be $y=Cx^m$ if there were no absorp-

tion. By assuming the loss mechanism described above, one can write the integral equation

$$y=Cx^m-a\int_0^x y(t)dt, \quad (\text{A1})$$

where a is a constant. This integral equation is of the type known as Volterra's linear integral equation of the second kind; the solution may be obtained by successive substitutions.⁹ The solution obtained by this method may be written as

$$y=Cx^m A_m(ax), \quad (\text{A2})$$

where $A_m(ax)$ is the hypergeometric series

$$A_m(ax) = 1 - \frac{ax}{m+1} + \frac{(ax)^2}{(m+1)(m+2)} - \frac{(ax)^3}{(m+1)(m+2)(m+3)} + \dots \quad (\text{A3})$$

This series becomes the exponential series when $m=0$, i.e., when y is a constant if the absorption were absent.

⁹ W. Lovitt, *Linear Integral Equations* (Dover Publications, Inc., New York, 1950), p. 13.

Calculations of Finite-Amplitude Distortion.

Bill D. Cook, Research Assistant, Physics Department, Michigan State University, East Lansing, Michigan, U.S.A.

Abstract: The distortion of plane finite amplitude sound waves in a dissipative, non-dispersive medium can be calculated by an iterative process of allowing the wave to distort and then correcting for the absorption. Results of such calculations are presented.

In the last few years, there has been considerable interest in the problem of finite-amplitude sound waves in dissipative media, primarily, because of the excess absorption of these waves. Most theoretical attempts to calculate finite-amplitude distortion and, consequently, the absorption have not been entirely successful. The chief difficulty with these theoretical attempts, which are usually based on equations approximating the exact differential equations, is that the range of reliability usually extends only up to the neighborhood of the discontinuity distance as given by the dissipationless theory. However, from the phenomenological aspects of the problem, a simple model can be formulated from which solutions for greater distances can be calculated. In this paper, an outline of this model is given and some of the more interesting conclusions are noted.

This model basically consists of applying distortion and absorption mechanisms in an iterative manner. This model is based on two fundamental processes which describe the distortion and absorption mechanisms independently. The mechanism for the distortion is described by a change in phase velocity directly proportional to the particle velocity. This may be written as

$$c = c_0 + [(B/2A) + 1] u \quad (1)$$

where c_0 is the velocity of sound waves of infinitesimal amplitude and u is the instantaneous particle velocity. The terms A and B , which are constants for a given medium and a given temperature, are defined by the equation of state relating the instantaneous pressure p and density ρ in the following equation:

$$p = p_0 + A \left[\frac{\rho - \rho_0}{\rho_0} \right] + (B/2) \left[\frac{\rho - \rho_0}{\rho_0} \right]^2 \quad (2)$$

where the zero subscripts refer to the undisturbed medium. For this model it is assumed that only this linear change in phase velocity causes the wave to distort. This distortion is produced as points on the wave having larger values of particle velocity tend to overtake points of lesser values. (see Fig. 1).

The absorption mechanism is described by assuming that the rate of absorption may be obtained by calculating the absorption of each harmonic independently according to the amount of the harmonic present and to the square of the frequency of the harmonic. This assumes that the absorption mechanisms are linear. With these two mechanisms, the procedure for the calculation of finite-amplitude distortion is the following: assume an initial waveform $f(x)$ which may be described by a set of Fourier coefficients b_n ; allow the wave to distort while propagating a small distance, producing the function $f_1(x)$ described by the coefficients $b_{n,1}$; correcting

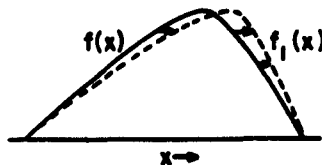


Figure 1.

coefficients for absorption; and then allowing these coefficients to describe the new waveform and continuing this process in an iterative manner. By assuming that the waveshape does not become multiple valued because of the absorption, one may calculate by this continuing process the shape of the wave at all distances. Although the generation and absorption of harmonics are treated independently in each interval, the end result contains the interaction between these mechanisms.

A model somewhat based on the same aspects outlined here was used by Fox and Wallace(1) in their attempt of calculating absorption coefficients for finite-amplitude waves. They graphically analysed the waveforms to obtain the Fourier coefficients. However, it is possible to use a parametric integration method for calculating the distortion process which allows the problem to be easily adapted to high speed computation. If the function $f(x)$ is known analytically, the function $f_1(\theta)$ may be obtained by introducing $x = \theta + k f(\theta)$ into $f(x)$. The term $k f(\theta)$ introduces the distortion mechanism required by Eq. 1. The quantity k represents the distance the wave has propagated in the interval in terms of the fractional distance to the discontinuity distance L for an initially sinusoidal wave. Introduction of the parameter θ allows the coefficients $b_{n,1}$ to be calculated from

$$b_{n,1} = \frac{2}{\pi} \int_0^{\pi} \{f(\theta) \sin [n\theta + nk f(\theta)] [1 + k f'(\theta)] d\theta \quad (3)$$

The discontinuity distance L represents the distance which initially sinusoidal waveform travels in a dissipationless medium before becoming multiple valued. At this distance, the wavefront has an infinite slope, however, the peak has moved only the distance of one radian with respect to the zero points of the wave. The distance L is given by

$$L = c_0^2 \left\{ 2[(B/2A) + 1] U_1(0) \pi f \right\}^{-1} \quad (4)$$

where f is the frequency of the wave and $U_1(0)$ is the maximum particle velocity of the initial sinusoidal wave. For this model, this distance L is sufficient to describe the distortion mechanisms and, consequently, is an important parameter in describing the results.

The absorption coefficient α of a wave of infinitesimal amplitude with the frequency of the fundamental component completely describes the absorption mechanism; hence, it is another important parameter for this model. Each harmonic is absorbed essentially exponentially for each interval in each iteration. The property of heat-conducting, viscous media having an absorption coefficient dependent on the square of the frequency is also taken into account.

Using the model previously described, calculations were made using a high speed electronic computer. To accurately retain the shape of the waveform, as many as $\frac{U_n(k)}{U_1(0)}$ sixteen harmonics were computed. The value of k , the length of each iteration was taken to be 0.05, one twentieth of the discontinuity distance. The results are presented in terms of the dimensionless product αL which adequately describes both distortion and absorption mechanisms. This parameter αL is related to the inverse of the Reynolds number.

This model is not expected to be valid for extremely intense sound waves which may produce periodic shock fronts but rather for sound waves of moderate amplitudes travelling in a fairly absorbing medium. The results presented are within these limitations.

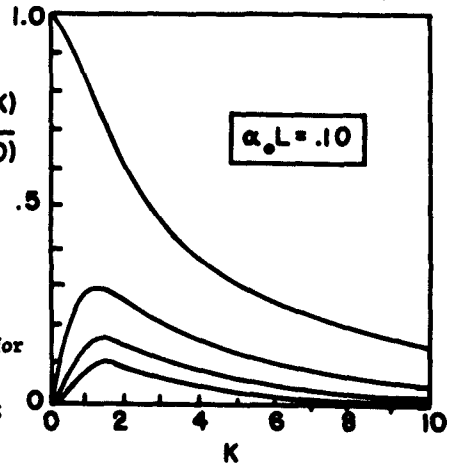


Figure 2.

Figure 3.

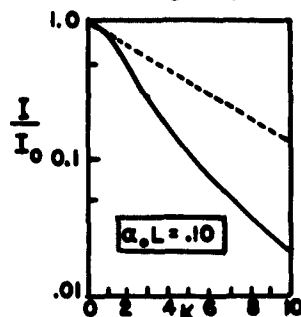


Figure 4.

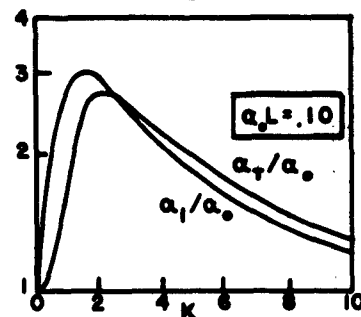


Figure 2 shows typical results from calculations made from this model. The amplitude of the particle velocity $U(K)$ of the harmonics are normalized to the amplitude $U_1(0)$ of the initial sinusoidal wave. The value of αL equals 0.10 for these curves. The abscissa, capital K , measures the distance the wave travels in units of the discontinuity distance. It is to be particularly noted that these calculations extend to 10 times the discontinuity distance. For these calculations, the amplitudes of the higher harmonics have their peak in the region where K is between 1 and 2.

Figure 3 shows the effect of the nonlinear propagation on the dissipation of the sound intensity calculated from the previous curves. As expected, there is a large difference between the exponential decay (dashed line) and the decay predicted by this model (solid line). The predicted greater absorption is, of course, caused by the higher rate of absorption of the generated harmonics. To describe this higher rate of absorption, one may define a finite amplitude absorption coefficient as

$$\alpha_T = -\frac{1}{2I} \frac{dI}{dx} \quad (5)$$

This coefficient describes the rate at which the energy of the total wave is being dissipated at any given distance. One may similarly define a coefficient α_1 for the energy carried by the fundamental component as

$$\alpha_1 = -\frac{d(U_1^2)}{2U_1^2 dx} \quad (6)$$

The absorption coefficient α_1 measures the rate of loss of energy from the fundamental component alone while α_T measures that from the total wave.

Figure 4 shows these coefficients (normalized to α_0) for the parameter $\alpha_0 L = 0.10$. It is important to note that the absorption coefficient α_1 for the fundamental frequency differs from the total absorption coefficient α_T for most values of K . It can be concluded that the total absorption coefficient can not be always obtained by measurements of the fundamental component only. The differences between α_1 and α_T can be very large at small distances where the energy carried by the fundamental is being lost by both distortion and absorption, while the energy of the total wave is being lost only by absorption.

As the results depend on the parameter $\alpha_0 L$, it is interesting to investigate the dissipation of the intensity as a function of this parameter. Figure 5 shows a semi-logarithmic plot of the

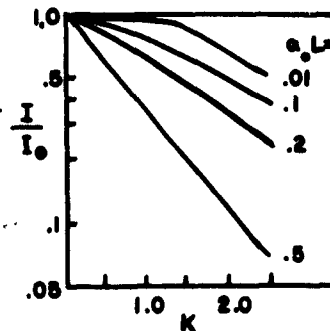


Figure 5.

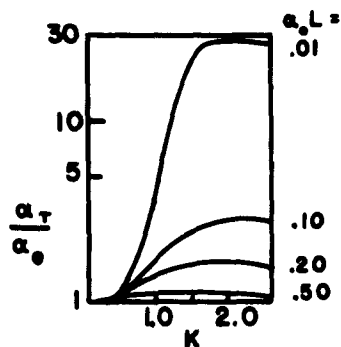


Figure 6.

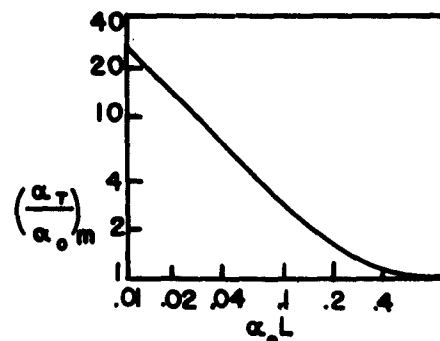


Figure 7.

intensity for different values of αL . For large values of $\alpha L (> 0.5)$, where the absorption is large or where the nonlinear effects are small, the decay is nearly exponential as the lower curve in Figure 5 is almost a straight line. In these cases, the wave is absorbed so fast that the nonlinear effects do not become appreciable. Hence, there is little or no excess absorption. For smaller values of αL , the wave becomes appreciably distorted and the excess absorption becomes noticeable. The upper-most curve of Figure 5 shows that the excess absorption becomes prominent after the wave has propagated to the vicinity of the discontinuity distance.

The differential absorption coefficient α_e gives a more detailed view of the rate of absorption. Figure 6 shows the absorption coefficients corresponding to the curves in Figure 5. For the smaller values of αL , the absorption coefficients have their maxima in the vicinity of $K = 1.6 L$. This corresponds to the situation that the peak of the initial wave moves $\pi/2$ with respect to the zero points of the wave. Physically, the movement of this peak is limited to this range as the particles cannot move through each other.

In Figure 7 the maximum values obtained by the absorption coefficient are plotted as a function of αL . For values of large $\alpha L (> 1)$, the finite amplitude distortion is completely negligible. For small values of αL , i.e., large nonlinear effects, the maximum absorption becomes inversely proportional to the parameter αL . In other words, at large sound pressures, the maximum absorption coefficient is directly proportional to the initial sound pressure. The nature of the curve in Figure 7 agrees somewhat with the theoretical results as outlined in the review paper of Zarembo and Krasil'nikov (2).

Although this model approach is an over simplification of the problem of finite-amplitude distortion, the results obtained from it are beneficial in understanding some of the properties of finite-amplitude distortion. At present there is not a sufficient amount of experimental data to check the range of validity of the results obtained using this model. (This work was supported by the Office of Naval Research, U.S. Navy and the U.S. Army Research Office (Durham)).

References.

1. F. E. Fox and W. A. Wallace, J. Acoust. Soc. Am. 26, 994-1006 (1954).
2. E. K. Zarembo and V. A. Krasil'nikov, Soviet Physics-Uspakhi 2, 580-599 (1959).

Optical Effects of Ultrasonic Waves Producing Phase and Amplitude Modulation

L. E. HARGROVE*

Department of Physics, Michigan State University, East Lansing, Michigan

(Received June 18, 1962)

A theory is developed for the diffraction of light by ultrasonic waves of sufficiently high frequency, large amplitude, and/or large beamwidth that the emerging light wavefront is significantly amplitude modulated in addition to the phase modulation considered in the Raman-Nath approach. The ultrasonic beam is considered to consist of N adjacent sections and the final diffraction spectrum to result from N successive diffractions. The diffraction orders emerging from a given section are considered to be sources for further diffraction by the next section. Only phase modulation of the separate plane waves (diffraction orders) is considered within a section. Refraction of light is not considered as such; it is characterized by successive redistribution of light in the diffraction orders. Numerical results are obtained by iterations using an electronic computer. These results are compared with measurements.

INTRODUCTION

THE diffraction of light by ultrasonic waves has been the subject of numerous experimental and theoretical investigations. Raman and Nath¹ developed a theory for conditions under which the ultrasonic frequency, amplitude, and/or beamwidth are sufficiently small that the *refraction* of light within the ultrasonic beam may be neglected. Under such conditions the ultrasonic beam may be considered to act as a pure *phase* grating producing only changes in the relative phase of the initially plane incident light wave and no intensity changes. The Raman-Nath approach has proven useful over a limited range. Herein, the Raman-Nath theory and other theories based on the phase

grating concept are called the Raman-Nath approach for sake of brevity.

When the ultrasonic frequency, amplitude, and/or beamwidth become large, refraction causes significant amplitude modulation along the emerging light wavefront. Extermann and Wannier,² Wagner,³ Van Cittert,⁴ and Mertens⁵ have obtained solutions for such conditions. Their results contain varying degrees of approximation and complexity.

In this paper, a solution to the problem of diffraction of light by sinusoidal, plane, progressive, ultrasonic waves is presented. The ultrasonic beam is considered to consist of N adjacent ultrasonic beams. For N

* Present address: Bell Telephone Laboratories, Inc., Murray Hill, New Jersey.

¹ C. V. Raman and N. S. Nath, Proc. Indian Acad. Sci. A2, 406-412 (1935); A3, 75-84 (1936).

² R. Extermann and G. Wannier, Helv. Phys. Acta. 9, 520-532 (1936).

³ E. H. Wagner, Z. Physik 141, 604-621 (1955).

⁴ P. H. Van Cittert, Physica 4, (1937).

⁵ R. Mertens, Mededel. Koninkl. Vlaam. Acad. Wetenschap. Belg. 12, 1-37 (1950).

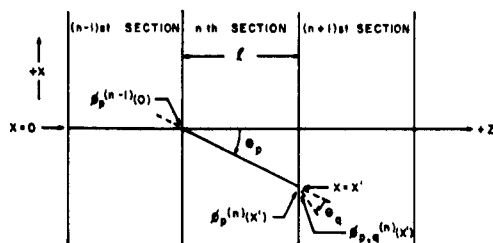


FIG. 1. Schematic diagram showing a diffraction order with amplitude $\phi_p^{(n-1)}(0)$ from the $(n-1)$ st section incident at $x=0$ on the n th section with angle of incidence θ_p ; sound propagation in the $+x$ direction, incident light in the $+s$ -direction.

sufficiently large only phase modulation of the light wavefronts need be considered *within* each of the N intervals. The final diffraction spectrum is considered to result from N successive diffractions.

THEORY

Consider, as indicated in Fig. 1, a section within the ultrasonic beam having thickness l assumed to be sufficiently small that refraction of light within the distance l may be neglected. Let this be the n th of many identical sections making up the whole ultrasonic beam. Diffraction orders emerging from the $(n-1)$ st section may be considered sources for further diffraction by the n th section. Figure 1 schematically represents the following situations: A diffraction order with amplitude $\phi_p^{(n-1)}(0)$ from the $(n-1)$ st section is incident at $x=0$ on the n th section with angle of incidence θ_p . Neglecting refraction, the incident light undergoes a change in phase on progressing through the n th section. This change is expressed by⁶

$$\phi_p^{(n)}(x') = \phi_p^{(n-1)}(0) \exp \left[\frac{-2\pi i}{\lambda} \int_0^{l/\cos\theta_p} \mu(s) ds \right], \quad (1)$$

where the integral in Eq. (1) represents the optical path through the n th section, λ is the wavelength of light *in vacuo*, and $\mu(s)$ expresses the refractive index along the light path. Using

$$\mu(s) = \mu_0 + \mu \sin 2\pi \left[(s \sin \theta_p - x') / \lambda^* \right], \quad (2)$$

where λ^* is the wavelength of sound and the Raman-Nath parameter $v_1 = 2\pi\mu l / \lambda$,

Eq. (1) becomes

$$\begin{aligned} \phi_p^{(n)}(x') = & \phi_p^{(n-1)}(0) \exp \left(\frac{-2\pi i \mu_0 l}{\lambda \cos \theta_p} \right) \\ & \times \exp \left\{ \left(\frac{-v_1 \lambda^*}{l \sin \theta_p} \right) \sin \left[2\pi \frac{(\frac{1}{2} l \tan \theta_p - x')}{\lambda^*} \right] \right. \\ & \left. \times \sin \left(\frac{\pi l \tan \theta_p}{\lambda^*} \right) \right\}. \quad (4) \end{aligned}$$

⁶ In this development the time dependence of the light and sound are not included, with the result that the Doppler shifts of the various diffraction orders are not shown. The small Doppler shift is neglected in writing the coefficient of the integral in Eq. (1).

Using the identity
 $\exp(-ia \sin b) =$

$$= \exp[ia \sin(-b)] = \sum_{q=-\infty}^{+\infty} J_q(a) \exp(-iqb), \quad (5)$$

Eq. (4) may be expressed in the form

$$\begin{aligned} \phi_p^{(n)}(x') = & \phi_p^{(n-1)}(0) \exp \left(\frac{-2\pi i \mu_0 l}{\lambda \cos \theta_p} \right) \\ & \times \sum_{q=-\infty}^{+\infty} J_q \left[\frac{v_1 \lambda^*}{l \sin \theta_p} \sin \left(\frac{\pi l \tan \theta_p}{\lambda^*} \right) \right] \\ & \times \exp \left[-2\pi i q \frac{(\frac{1}{2} l \tan \theta_p - x')}{\lambda^*} \right]. \quad (6) \end{aligned}$$

In Eq. (6) a term for a particular q represents light incident on the n th section at an angle θ_p , and incident on the $(n+1)$ st section at an angle $\theta_p + \theta_q$, where

$$\sin \theta_q = -k\lambda / (\mu_0 \lambda^*). \quad (7)$$

Consider one such component (particular p and q) from Eq. (6) denoted by $\phi_{p,q}^{(n)}(x')$. This relates a particular emerging component at x' to the one, namely $\phi_p^{(n-1)}(0)$, incident on the n th section at $x=0$. In order that each successive section may be treated in mathematically identical manners, $\phi_{p,q}^{(n)}(x')$ must be transformed to $\phi_{p,q}^{(n)}(0)$ in order that the point of incidence on the $(n+1)$ st section will also be at $x=0$.

The transformation from x' to $x=0$ involves an ultrasonic phase shift and an optical phase shift as indicated in Fig. 2. The effect of an ultrasonic phase shift is expressed by a factor $\exp(-ip\delta^*)$, where δ^* is the ultrasonic phase difference. From Fig. 2 it is seen that

$$\exp(-ip\delta^*) = \exp(2\pi i p l \tan \theta_p / \lambda^*). \quad (8)$$

Similarly, the effect of the optical phase shift is expressed by a factor

$$\begin{aligned} \exp(-i\delta) = & \exp(2\pi i \mu_0 l \tan \theta_p \sin \theta_p / \lambda) \\ = & \exp(-2\pi i p l \tan \theta_p / \lambda^*), \quad (9) \end{aligned}$$

where δ is the optical phase difference and Eq. (7) has been used. The transformation then consists of multi-

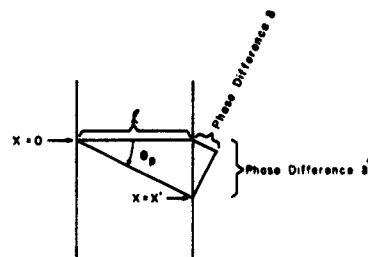


FIG. 2. Schematic diagram illustrating the optical and ultrasonic phase differences involved in transforming from $x=x'$ to $x=0$.

plying $\phi_{p,q}^{(n)}(x')$ by the right-hand members of Eqs. (8) and (9). Noting that these two factors are simply complex conjugates, and that their product is unity, then

$$\phi_{p,q}^{(n)}(0) = \phi_{p,q}^{(n)}(x'). \quad (10)$$

Having transformed the separate components corresponding to various p and q to a common point $x=0$, the components propagating in a given direction may be combined to obtain the amplitudes of the diffraction orders which act as new sources for further diffraction in the $(n+1)$ st section. The terms to be combined to obtain the amplitude of the r th order are those for which $p+q=r$, i.e.,

$$\phi_r^{(n)} = \sum_{p=-\infty}^{+\infty} \phi_p^{(n-1)} J_{r-p} \left[\frac{v_l \lambda^*}{l \pi \sin \theta_p} \sin \left(\frac{\pi l \tan \theta_p}{\lambda^*} \right) \right] \times \exp \left[\frac{-2\pi i \mu_0 l}{\lambda \cos \theta_p} \right] \exp \left[\frac{\pi i (r-p) l \tan \theta_p}{\lambda^*} \right], \quad (11)$$

where x' has been expressed by

$$x' = l \tan \theta_p. \quad (12)$$

Equation (11) expresses an iterative procedure for calculating the final diffraction order amplitudes $\phi_r^{(N)}$ resulting from N successive diffractions.

Equation (11) may be put into an approximate form which is more suitable for numerical evaluation. Using the approximations

$$\tan \theta_k \approx \sin \theta_k = -k\lambda / (\mu_0 \lambda^*), \quad (13)$$

$$1/\cos \theta_k = \sec \theta_k \approx 1 + \frac{1}{2} \theta_k^2, \text{ where } \theta_k \approx \sin \theta_k, \quad (14)$$

and introducing the parameter⁷

$$Q_l = (2\pi\lambda l) / (\mu_0 \lambda^{*2}), \quad (15)$$

Eq. (11) becomes

$$\phi_r^{(n)} = \sum_{p=-\infty}^{+\infty} \phi_p^{(n-1)} J_{r-p} \left(\frac{v_l \sin \frac{1}{2} p Q_l}{\frac{1}{2} p Q_l} \right) \times \exp(-\frac{1}{2} i p r Q_l). \quad (16)$$

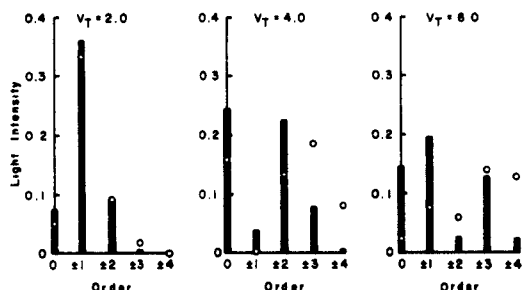


FIG. 3. Light intensities predicted by the present theory (vertical bars) for $Q_T=1.5$, using Q_T' in Eq. (16) and by the Raman-Nath theory (circles).

⁷The parameter Q appears in some form in various other theories for the diffraction of light by ultrasonic waves.

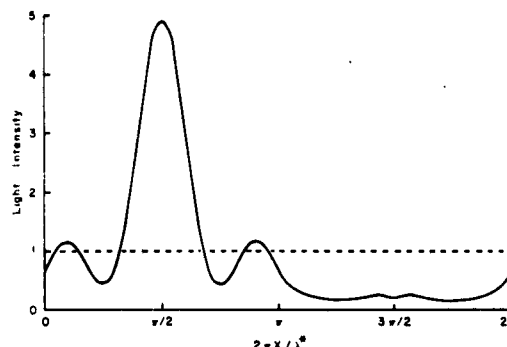


FIG. 4. Intensity modulation of the light wavefront emerging from the ultrasonic beam for $v_T=4$ and $Q_T=1.5$, using Q_T' .

In either Eq. (11) or Eq. (16)

$$\phi_0^{(0)} = 1, \quad \phi_{p \neq 0}^{(0)} = 0, \quad (17)$$

and

$$\phi_p^{(1)} = J_p(v_l) \quad (18)$$

for unit incident-light amplitude and normal light incidence. The light intensities in the final spectrum are obtained from

$$I_r = |\phi_r^{(N)}|^2. \quad (19)$$

It has been assumed that the refraction of diffraction orders within each section may be neglected and the Raman-Nath approach applied therein. Limitations on Q and v for validity of the Raman-Nath approach have been given in the form²

$$Qv \ll 2. \quad (20)$$

The degree of inequality required in (20) depends on the accuracy required. It is proposed that the number of sections chosen for application of the present theory be sufficiently large that $(Qv)_i$ be less than two by a factor of one or two orders of magnitude. The number of sections N may be increased as required to obtain theoretical results for large Q_T and v_T pertaining to the total ultrasonic beam.

Straightforward application of the present theory would require that

$$l = L/N, \quad (21)$$

where L is the total width of the ultrasonic beam, be used in Eqs. (3) and (15) which define v_l and Q_l which appear in Eq. (16). However, an alternative approach is proposed. Note, in Eq. (18), that in the first section the result is independent of Q . Refraction effects, as characterized by spreading of light into the various diffraction orders as it emerges from each successive section, are in no way considered in the first section. If the ultrasonic beam width L were divided into twice as many sections, refraction effects would be ignored in a first section of half the width. In order to approxi-

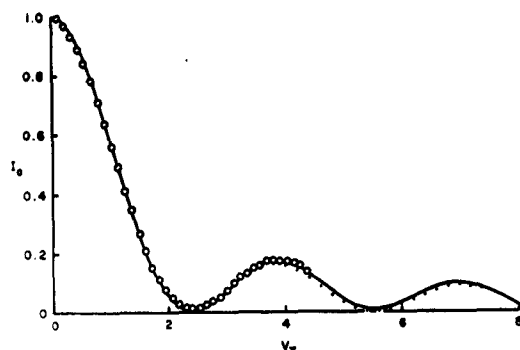


FIG. 5. Theoretical (line) and experimental (circles) zeroth-order light intensity vs Raman-Nath parameter for $Q_T=0.62$, using Q_T' .

mately account for refraction effects in a first interval of finite width, it is proposed that

$$Q_T' = Q_T / (N - 1) \quad (22)$$

be used in Eq. (16) to replace Q_T . The Raman-Nath parameter v_i should remain as

$$v_i = v_T / N. \quad (23)$$

Use of Eq. (22) is equivalent to using

$$Q_T' = Q_T N / (N - 1) \quad (24)$$

as an "effective Q " to compensate for use of finite sections of the ultrasonic beam. Obviously, as the number of sections N becomes very large, the difference between Q_T' and Q_T vanishes.

NUMERICAL RESULTS AND COMPARISON WITH EXPERIMENTAL DATA

Numerical calculations were made from Eq. (16) using the Michigan State Integral Computer (MISTIC). The choice of $0 \leq v_T \leq 8$, $Q_T \leq 1.5$, and $N = 16$ gives $(Qv)_i < 0.05$. The value $N = 16$ was also chosen for convenience in a binary computer. Calculations were made for 0.25 intervals of v_T and for p (and therefore also r)

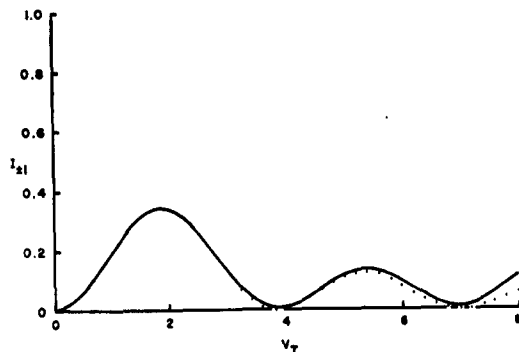


FIG. 6. Theoretical first-order light intensity vs Raman-Nath parameter for $Q_T=0.62$, using Q_T' .

ranging from -4 to $+4$. For a given range of v_T the range of p should be taken over values for which significant light occurs in the p th orders. The final results are probably less reliable as $|r|$ approaches the maximum $|p|$ used.

The differences between predictions of the present theory and the Raman-Nath theory are illustrated in Fig. 3. The predicted light intensities in the zeroth through fourth diffraction orders are shown for $Q_T = 1.5$, using Q_T' in Eq. (16), for $v_T = 2, 4$, and 6.

Using the calculated amplitudes and phases of the diffraction orders, the calculated intensity modulation of the light wavefront emerging from the ultrasonic beam for the $v_T = 4$ case shown in Fig. 3 is shown in Fig. 4. Note that the intensity modulation is quite significant. This intensity modulation explains the failure of the Raman-Nath theory for this case where $(Qv)_T = 6$. Taking the refraction viewpoint, concentration of light about $\frac{1}{2}\pi$ indicates light refracted toward this region where the density of the medium and hence the refractive index is greatest.

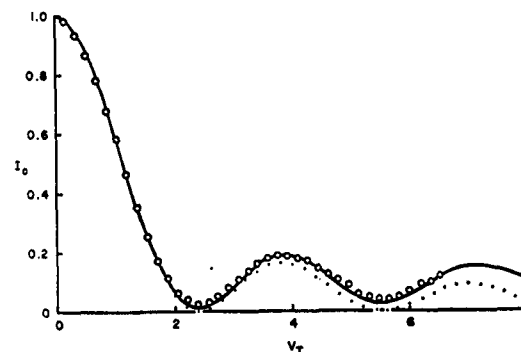


FIG. 7. Theoretical and experimental zeroth-order light intensity vs Raman-Nath parameter for $Q_T=0.93$, using Q_T' .

Figures 5 through 10 show calculated zeroth- and first-diffraction-order light intensities for $Q_T = 0.62, 0.93$, and 1.24, using Q_T' in Eq. (16). The predictions of the Raman-Nath theory are also shown in these figures, where clarity permits. Experimental results for the indicated values of Q_T , obtained by Klein,⁸ are also shown in Figs. 5 and 7 through 10. Klein's measurements were made at 5.23 Mc in water. Q_T was varied by varying the ultrasonic beam width (2.0, 3.0, and 4.0 cm for the data shown).

Klein found good agreement between Mertens's⁸ theory and his experimental values of light intensity in the zeroth and first diffraction order,⁸ for a limited range of Q_T and v_T . The present theory agrees with the Mertens theory where the Mertens theory is in reasonable agreement with measurements. However, the present theory appears to be valid over a wider range of Q_T and v_T .

⁸ W. R. Klein, M. S. thesis, Michigan State University (1962).

For comparison, the zeroth-order light intensities predicted by the present theory (using both $Q_T=1.5$ and $Q_T'=1.5(N/N-1)$ for calculations), by the Mertens' theory for $Q_T=1.5$, and by the Raman-Nath theory are shown in Fig. 11. If the present theory is valid, then the Mertens' theory is a good approximation, in this case, for $v_T \leq 4.0$. The difference between the curves in Fig. 11 for the present theory using Q_T and Q_T' is not great, but the difference is generally in the correct sense to give better agreement with experimental values by using Q_T' .

Calculations have been made for $Q_T=0.31$ and compared with the predictions of the Raman-Nath theory. The predicted light intensities in the diffraction orders agree to within 0.01 up to the values of v_T indicated in Table I. This agreement over a fairly large range of v_T demonstrates that the method of calculation used in the present theory gives results which approach the Raman-Nath results for a small value of Q_T .

It should be pointed out, however, that only agreement in light intensity has been obtained for $Q_T=0.31$. The relative optical phases should also be considered. The intensity modulation of the emerging light wavefront shown in Fig. 4 for $Q_T=1.5$ results not only from light amplitudes which differ from those predicted by

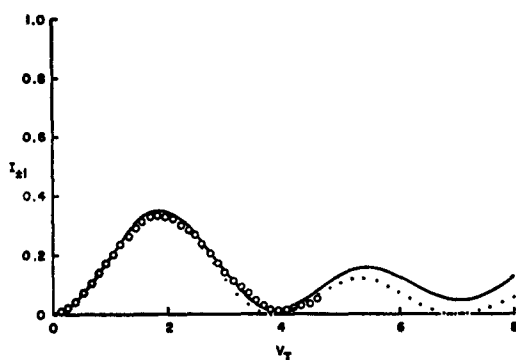


FIG. 8. Theoretical and experimental first-order light intensity vs Raman-Nath parameter for $Q_T=0.93$, using Q_T' .

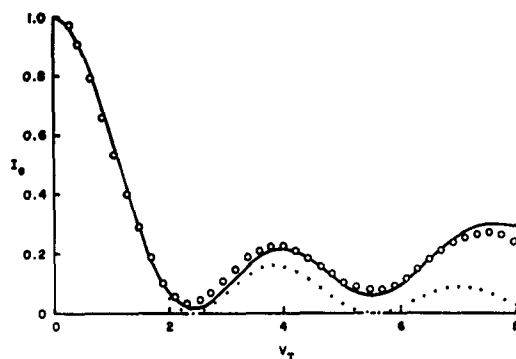


FIG. 9. Theoretical and experimental zeroth-order light intensity vs Raman-Nath parameter for $Q_T=1.24$, using Q_T' .

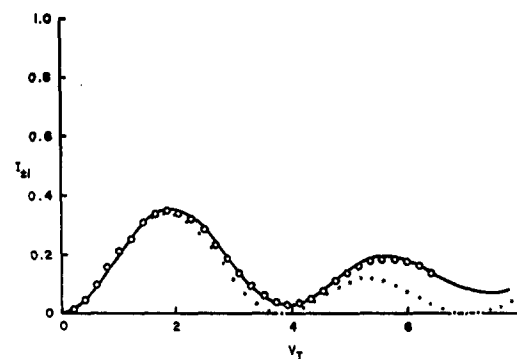


FIG. 10. Theoretical and experimental first-order light intensity vs Raman-Nath parameter for $Q_T=1.24$, using Q_T' .

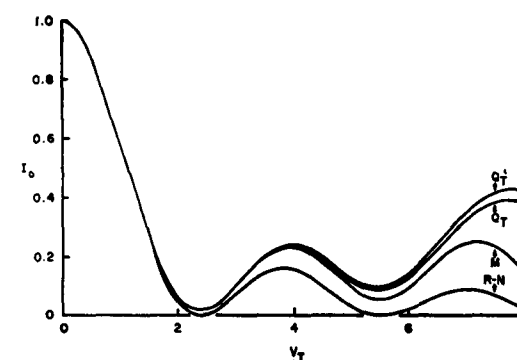


FIG. 11. Zeroth-order light intensities vs Raman-Nath parameter from present theory (using both $Q_T=1.5$ and $Q_T'=1.5(N/N-1)$), Mertens' theory for $Q_T=1.5$, and Raman-Nath theory.

the Raman-Nath theory, but also from different relative phases of the various diffraction orders. The relative phases in the Raman-Nath theory are either 0 or π rad, according to whether the Bessel function is positive or negative, respectively. The calculations for $Q_T=0.31$, though the light intensities agree with the Raman-Nath theory, show marked deviations in relative phase from 0 or π rad. This indicates that the Raman-Nath theory may appear satisfactory from intensity measurements but not be accurate where the relative phases are concerned. The relative phases become important, as pointed out in a previous paper,⁹ in a situation involving successive diffraction of light by two separate ultrasonic beams.

TABLE I. Maximum values of v_T for which the predictions of the present theory and the Raman-Nath theory agree to within 0.01 light intensity. $Q_T=0.31$.

| Order | 0 | ± 1 | ± 2 | ± 3 | ± 4 |
|-------|-----|---------|---------|---------|---------|
| v_T | 7.0 | >8 | 7.25 | 6.0 | 4.0 |

⁹ L. E. Hargrove, E. A. Hiedemann, and R. Mertens, *Z. Physik* 167, 326-336 (1962).

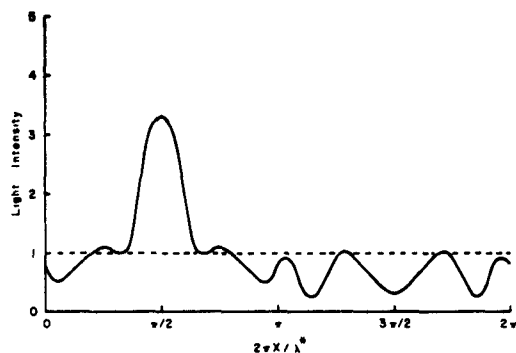


FIG. 12. Intensity modulation of the light wavefront emerging from the ultrasonic beam for $V_T=4$ and $Q_T=0.31$, using Q_T' .

The agreement in intensity predictions may also be considered to demonstrate that the Raman-Nath approach predicts the correct intensities even when there is some degree of light intensity modulation along the emerging light wavefront. Figure 12 shows the intensity modulation calculated for $Q_T=0.31$ and $v_T=4.0$. It has been shown in Table I that the present theory and the Raman-Nath theory give essentially the same light intensities through fourth orders up to this value of v_T . Therefore, the intensity modulation shown in Fig. 12 is an estimate of the upper limit of intensity modulation for which the Raman-Nath theory gives the correct light intensities in the first four diffraction orders. Figures 4 and 12 are for the same value of v_T but

different Q_T , and may be compared to illustrate the difference in intensity modulation for ultrasonic beams with the same "diffraction strength" v_T but different Q_T . Finally, it is remarked that the light intensity modulation for the smallest $(Qv)_T$ calculated ($Q_T=0.31$ and $v_T=0.25$, giving $(Qv)_T \approx 0.08$) deviates from unity by at most approximately 0.04.

DISCUSSION

The predictions of the present theory are in good agreement with Klein's experimental data. The agreement is somewhat better, for the larger values of Q_T and v_T , than that found by Klein using Mertens' theory.

Diffraction of light by high-frequency, intense, ultrasonic waves is of particular interest for determining the waveform of distorted finite-amplitude waves in liquids. While the present results are restricted to sinusoidal waves, work is in progress to extend the theory to include arbitrary ultrasonic waveform, especially waveforms of the finite-amplitude type.

ACKNOWLEDGMENTS

The author wishes to thank Professor E. A. Hiedemann for the interest he has shown in this work. Credit is due B. D. Cook, who suggested the successive diffraction approach to the present problem.

This work was supported by the U. S. Army Research Office (Durham) and by the Office of Naval Research.

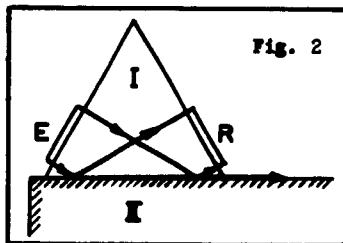
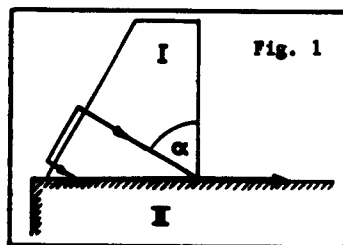
ON THE CONVERSION OF LONGITUDINAL TO SURFACE WAVES IN SOLIDS

Walter G. Mayer

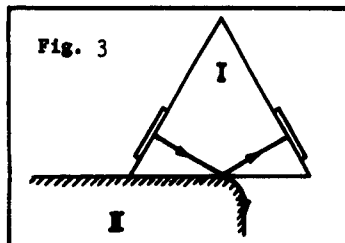
Physics Department, Michigan State University,
East Lansing, Michigan, U.S.A.

Various experimental techniques for the production of surface waves on a free surface of a solid have been described in the past (1). Quite frequently one uses the method of converting a longitudinal wave in a solid to a surface wave on another solid in contact with the first. The present paper is concerned with this type of mode conversion because the energy transfer from a longitudinal to a surface wave seems to offer possibilities for decreasing the intensity of the reflection of the longitudinal wave in the solid through which it is propagated. Some experimental results for a specific case are given here.

The production of a surface wave is usually accomplished by the familiar wedge method shown in Figure 1. The amplitude of the surface wave reaches a maximum (2) when the angle of incidence α is chosen that the ratio $V_L/V_S = \sin\alpha$, where V_L is the velocity of the longitudinal wave in solid I, and V_S is the velocity of the surface wave on solid II. An arrangement of this type has the disadvantage that one cannot easily determine how much energy contained in the longitudinal wave is transferred to the surface wave. A slightly different wedge was therefore used, shown in Figure 2. An ultrasonic pulse is emitted by transducer E. If the bottom surface of the wedge is in contact with air the pulse will be totally reflected and will be picked up by the receiving transducer R. The amplitude of the received pulse is taken as reference for the subsequent experiment in which the wedge is placed on the smooth surface of solid II. In the experiments described here solid II is aluminum while solid I is Plexiglas. The velocities V_L and V_S were determined experimentally by a conventional pulse method. Placing the Plexiglas wedge on the aluminum surface allows the mode conversion from a longitudinal wave in the wedge to a surface wave on the aluminum. The wedge is cut in such a way that the angle of incidence α satisfies the above condition for optimum surface wave production. With the wedge on solid II there is no more total reflection of the incident pulse, and the amplitude of the signal received by transducer R should decrease by an amount determined by the energy converted to the surface wave. However, it is found that using the Plexiglas wedge the amplitude of the received pulse increases when the wedge is placed on the aluminum. This may be explained by considering the loss mechanisms. If the wedge is not in contact with solid II every part of the sound signal emitted by transducer E travels the same distance in the wedge before it reaches transducer R. The absorption in the Plexiglas is quite high. If the wedge is then placed on the aluminum a surface wave is generated between the two solids. As this wave propagates along the surfaces it may radiate energy back into the wedge. If the absorption of this wave should be less than the absorption of the longitudinal wave in the wedge a signal of higher amplitude would be received at R than if the signal had traveled entirely in the Plexiglas.

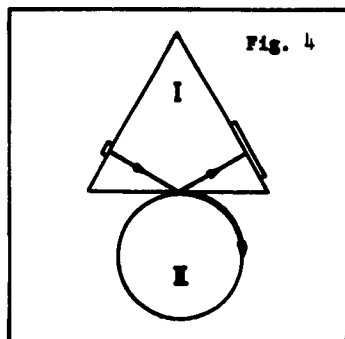


One would, therefore, like to minimize this radiation back into solid I. Ideally, one would like to separate the surface wave from the bottom of the wedge as soon as it is generated. But this wave is generated over a finite area of contact between the two solids, and the size of this area is determined by the size of the emitting transducer and the angle of incidence; one therefore encounters certain experimental limitations in separating the surface wave from the bottom of the wedge. Since the central portion of the ultrasonic signal emitted from transducer E contains more energy



than the outside of the beam one might remove the corresponding most intense portion of the surface wave by rounding off one edge of solid II and placing it in relation to the wedge as indicated in Figure 3. The radius of curvature of the rounded edge is big enough so that the surface wave will travel around it (3). Adjusting the relative positions of the wedge and solid II in this manner one transfers the most intense part of the longitudinal wave in the wedge to a surface wave which is then conducted away from the wedge, thus reducing radiation back toward the receiving transducer.

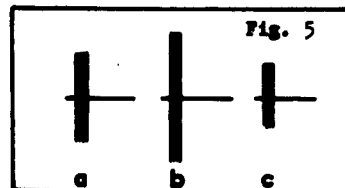
In order to decrease further the area of contact in which surface waves are generated one can decrease the dimensions of the emitting transducer. Doing this one narrows the width of the longitudinal wave impinging on solid II and one can reduce the received signal by replacing the aluminum block by a solid aluminum cylinder as shown in Figure 4.



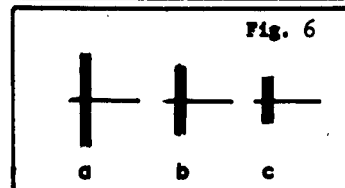
This reduces the area of contact between the two solids and assures a more efficient separation of the surface wave from the bottom of the wedge. Changing the size of the aluminum cylinder changes the effective area of contact and thus the amplitude of the received pulse. The angle of incidence α is not affected by the size of the cylinder.

The surface wave traveling around the cylinder is absorbed by placing some suitable liquid on the cylinder; if this is not done, the wave completes the circle and reaches the wedge again where it is converted back into a longitudinal wave which travels toward R. In this case one has a short delay line.

The efficiency of mode conversion from longitudinal to surface wave for the various arrangements described can be seen from the results of experiments using Plexiglas and aluminum. Using a 5 Mc pulse from a 1.2 x 2.5 cm transducer and placing the entire wedge on the aluminum one receives a signal whose amplitude is shown in Figure 5b.



The reference amplitude (wedge in air) is shown in Figure 5a. The amplitude of the signal has increased by about 50 percent; thus, placing the entire wedge on the aluminum block does not reduce the reflections back into the wedge. Figure 5c shows the received amplitude of the reflected longitudinal wave recorded with the arrangement indicated in Figure 3. In this case the amplitude has decreased somewhat. A more effective energy transfer is attainable if the wedge is placed on a solid aluminum cylinder. The received amplitude is indicated in Figure 6b, compared with the reference amplitude in Figure 6a (wedge in air). The diameter of the cylinder was 1.85 cm. The effective area of contact between the two solids was increased slightly by using a solid aluminum cylinder with a diameter of 6.34 cm. In this case the received signal had an amplitude shown in Figure 6c. The results shown in Figure 6 were ob-



tained by using an emitting transducer with dimensions 0.25×2.5 cm which minimized further the effective area of surface wave production. It is seen that the reflected longitudinal wave decreases to about half its amplitude in the last case shown in Figure 6.

This reduction in amplitude of the reflected longitudinal wave indicates that an appreciable part of the energy in the longitudinal wave can be taken out of solid I by mode conversion to a surface wave on solid II, especially if one considers that the greatest part of the cross-section of the sound beam is impinging on the Plexiglas-air interface and only a small part on the Plexiglas-aluminum interface. The resulting surface wave can be absorbed very easily so that it will not be reflected back into solid I. That fraction of the longitudinal wave in solid I which was not converted to

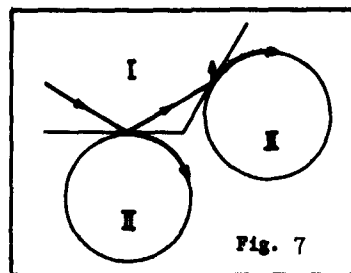


Fig. 7

a surface wave at the boundary can be reduced further by repeating the process as indicated in Figure 7. In principle, it should be possible to use this technique for the suppression of reflections of an ultrasonic wave in a solid. Since the absorption of the resulting surface wave presents no problem one should be able to approach the production of progressive ultrasonic waves in solids using the method outlined here, provided the velocity of the longitudinal wave in the solid in question is smaller than the velocity of the surface wave on solid II. (This work was supported by the Office of Naval Research, U.S. Navy.)

Bibliography

- (1) I. A. Viktorov, Soviet Phys.- Acoustics 7, 236 (1962).
- (2) E. G. Cook and H. E. Van Valkenburg, ASTM Bull. No. 198, 81 (1954).
- (3) I. A. Viktorov, Soviet Phys.- Acoustics 7, 70 (1961).

Reflection and Refraction of Mechanical Waves at Solid-Liquid Boundaries

by

Walter G. Mayer

Abstract.

The energy ratios of reflected and refracted waves to the incident wave at ten liquid-solid boundaries are calculated as a function of the angle of incidence. The influence of the wave velocities in the media and their density on the shape of the curves is discussed.

INTRODUCTION

Knowledge of the energy ratios between incident, reflected, and refracted mechanical waves at interfaces formed by two dissimilar media is of great importance in ultrasonics¹⁻³, seismology⁴, and for material testing techniques^{5,6}. Knott⁷ and Zoeppritz⁸ have given expressions describing the changes of amplitude of reflected and refracted waves as a function of the angle of incidence. Based on their work, Ergin⁴ has calculated these amplitude ratios for seismic waves incident at both sides of the ocean floor. Mayer and Kelsey³ have measured the velocities of ultrasonic waves in solids by observing the amplitudes of the reflected waves in the liquid. These measurements and the results given here allow one to draw a number of useful conclusions about the behavior of the reflected and refracted waves. However, Ergin considers only the changes in the energy ratios caused by a relatively small change in the ratio of the longitudinal to shear wave velocity (essentially the Poisson's ratio) of the solid medium. The present paper also considers the influence of the density ratio and the ratio of the longitudinal wave velocities of the two media.

RESULTS

The system under consideration consists of a liquid with density ρ_1 and a solid medium with density ρ_2 . The plane surface of the solid is in contact with the liquid. The velocity of the longitudinal wave in the liquid is V_{L1} . The velocity of the longitudinal wave in the solid is given by V_{L2} and that of the shear wave by V_{S2} . The energy of the incident wave in the liquid is unity, and the angle of incidence is denoted by α , measured from the normal to the liquid-solid boundary. According to Ergin⁴, the energy ratio of reflected to incident wave is given by

$$(R/I)^2 = \left(\frac{[\cos \beta - A \cos \alpha (1 - B)]}{[\cos \alpha + A \cos \alpha (1 - B)]} \right)^2, \quad (1)$$

where $A = V_{L2} \rho_2 / V_{L1} \rho_1$,

$$B = 2 \sin \gamma \sin 2\gamma [\cos \gamma - (V_{S2}/V_{L2}) \cos \beta].$$

The angles β and γ are the angles of refraction of the longitudinal and the shear wave in the solid, determined by Snell's law

$$V_{L1} / \sin \alpha = V_{L2} / \sin \beta = V_{S2} / \sin \gamma.$$

The energy ratio of refracted longitudinal wave in the solid to the incident wave in the liquid is given by

$$(L/I)^2 = \left(\frac{2 \cos 2\gamma (A \cos \alpha \cos \gamma)^{\frac{1}{2}}}{[\cos \beta + A \cos \alpha (1 - B)]} \right)^2. \quad (2)$$

The energy ratio of refracted shear wave to incident wave is then

$$(S/I)^2 = 1 - (R/I)^2 - (L/I)^2. \quad (3)$$

Calculations of these ratios were made for a number of solids with the incident wave in water and oil. The values of velocities and densities used are shown in Table I. Poisson's ratio σ is also shown.

Table I. Velocities and Densities Used for Calculations

| | V_{L1} | ρ_1 | V_{L2} | V_{S2} | ρ_2 | σ |
|-----------|----------|----------|----------|----------|----------|----------|
| Water | 1490 | 1.00 | | | | |
| Oil | 1740 | 0.87 | | | | |
| Steel | | | 5850 | 3230 | 7.80 | 0.281 |
| Brass | | | 4430 | 2123 | 8.10 | 0.351 |
| Copper | | | 4700 | 2260 | 8.90 | 0.350 |
| Aluminum | | | 6330 | 3130 | 2.70 | 0.338 |
| Magnesium | | | 5770 | 3050 | 1.70 | 0.306 |

Velocities in m/sec.

Since one cannot readily see from eqs. (1-3) how the intensity of the waves is influenced by changes in the various parameters, individual calculations were made for all the possible combinations of liquids and solids listed in Table I. The results are plotted in Figs. 1-5. The solid lines are for oil-solid interfaces, the dashed lines for water-solid interfaces. The letters R, L, and S denote the curves for the reflected longitudinal wave, the refracted longitudinal wave, and the refracted shear wave, respectively.

DISCUSSION

The general conclusions drawn from the curves in Figs. 1-5 are valid only if $V_{L2} > V_{S2} > V_{L1}$. This excludes boundaries formed by some liquids and plastics where $V_{S2} < V_{L1}$.

The ratio $(R/I)^2$ becomes unity at the critical angle for the refracted longitudinal wave ($\sin\beta = 1$) and again at the critical angle for the shear wave ($\sin\gamma = 1$). The location of these critical angles α_L and α_S depends only on the ratios V_{L2}/V_{L1} and V_{S2}/V_{L1} . Total reflection occurs at these angles of incidence regardless of the values of density and velocity.

The value of $(R/I)^2$ for normal incidence depends only on $V_{L1}\rho_1$ and $V_{L2}\rho_2$; eq. (1) reduces to the well-known formula for the reflection coefficient. The shear wave velocity is of no consequence at $\alpha = 0$.

The general behavior and the minima of the $(R/I)^2$ curve remains essentially the same if instead of given values for V_{L1} and ρ_1 one selects slightly different values without changing appreciably the acoustic impedance of the liquid medium (water and oil). This also holds for the maxima of the $(L/I)^2$ and $(S/I)^2$ curves.

Poisson's ratio is not a dominating factor in the behavior of the curves. Of the solids considered steel and magnesium have the lowest Poisson's ratios, yet, the curves for the other three substances lie between those for steel and magnesium.

The energy of the reflected wave is determined mainly by its value at $\alpha = 0$. The ratio $(R/I)^2$ stays almost constant until the critical angle for the refracted longitudinal wave is approached. The width of the peak at that angle depends on the energy at $\alpha = 0$ and on the cutoff angle for the shear wave. The peak is sharper the lower $(R/I)^2$ at $\alpha = 0$ and the smaller α_S . Beyond α_L the curve dips sharply and reaches a minimum which is always less than $(R/I)^2$ at $\alpha = 0$. This means that in certain solids a shear wave can be produced which is more intense than the reflected longitudinal wave (Fig. 5). Whether this is possible depends primarily on the acoustic impedances and to a lesser degree on the shear velocity.

The energy of the shear wave between $\alpha = 0$ and α_L is much smaller than its energy between α_L and α_S , the maximum depends strongly on the values of α_S and the width of the $(R/I)^2$ peak.

With this information, and since the two cutoff angles can be found easily from Snell's law and the initial values at $\alpha = 0$ from the reflection coefficient, it is possible to estimate the behavior of the three curves $(R/I)^2$, $(L/I)^2$, and $(S/I)^2$ for a given set of velocities and densities in the range considered here without having to make many time-consuming calculations.

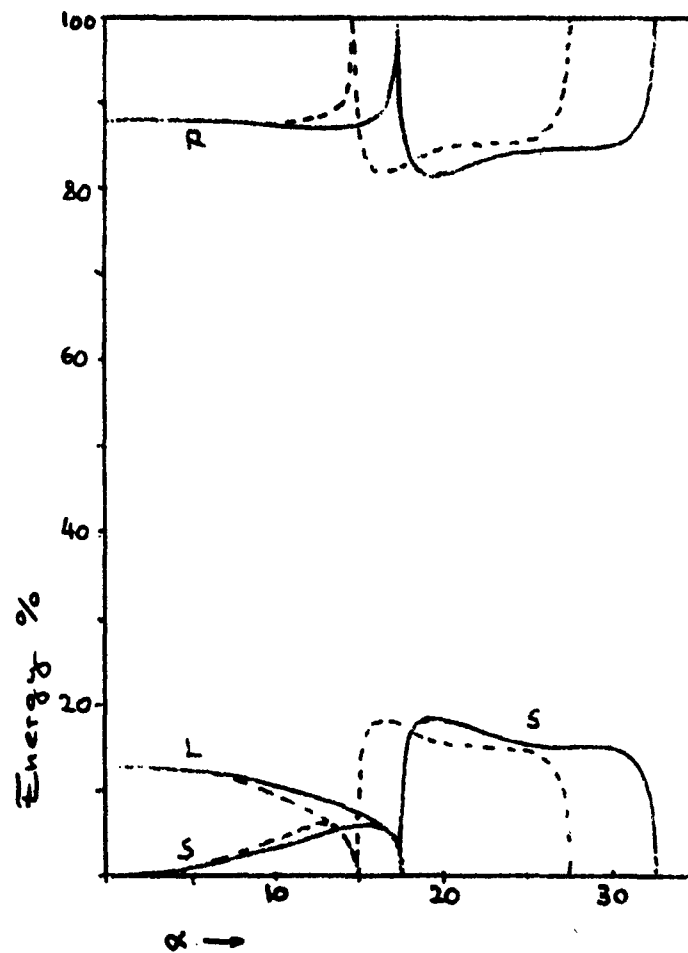


Figure 1. Energy relations at oil-steel boundary (solid lines) and water-steel boundary (dashed lines).

R reflected wave,
 L refracted longitudinal wave,
 S refracted shear wave.

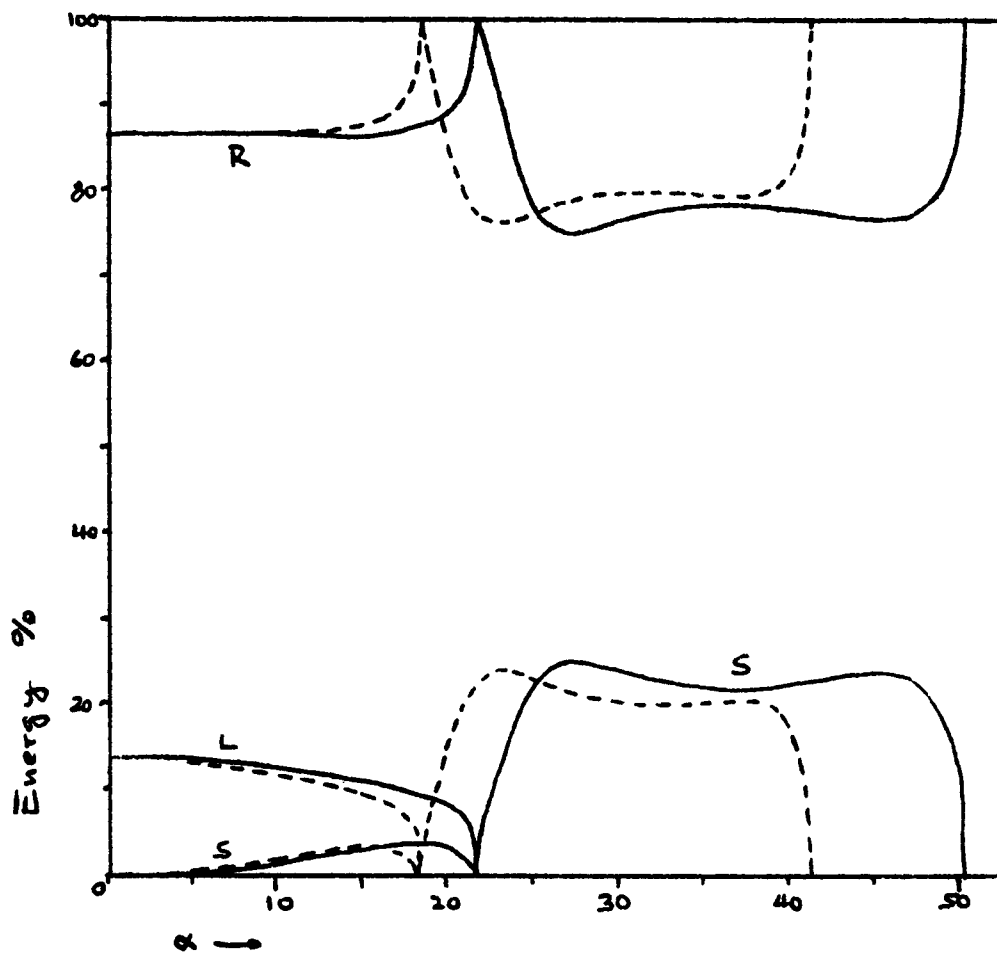


Figure 2. Same as Fig. 1 for copper.

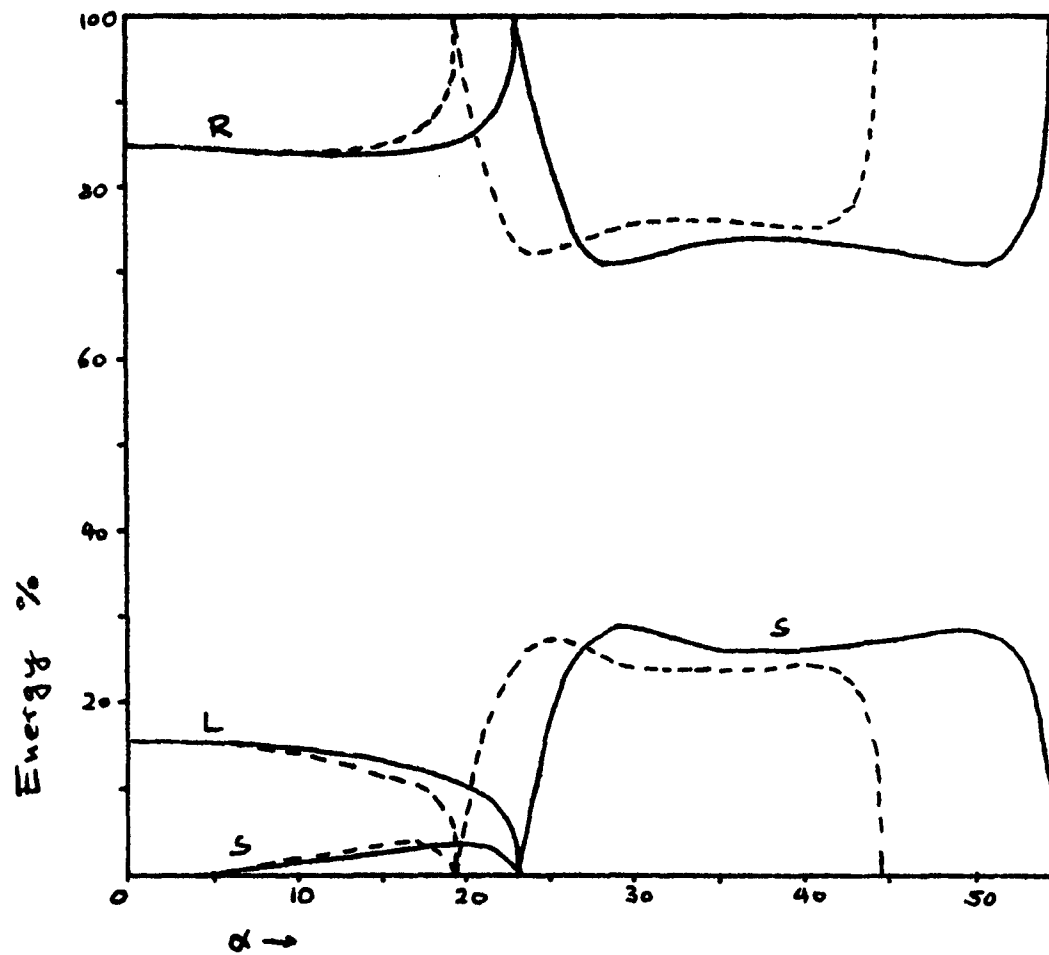


Figure 3. Same as Fig. 1 for brass.

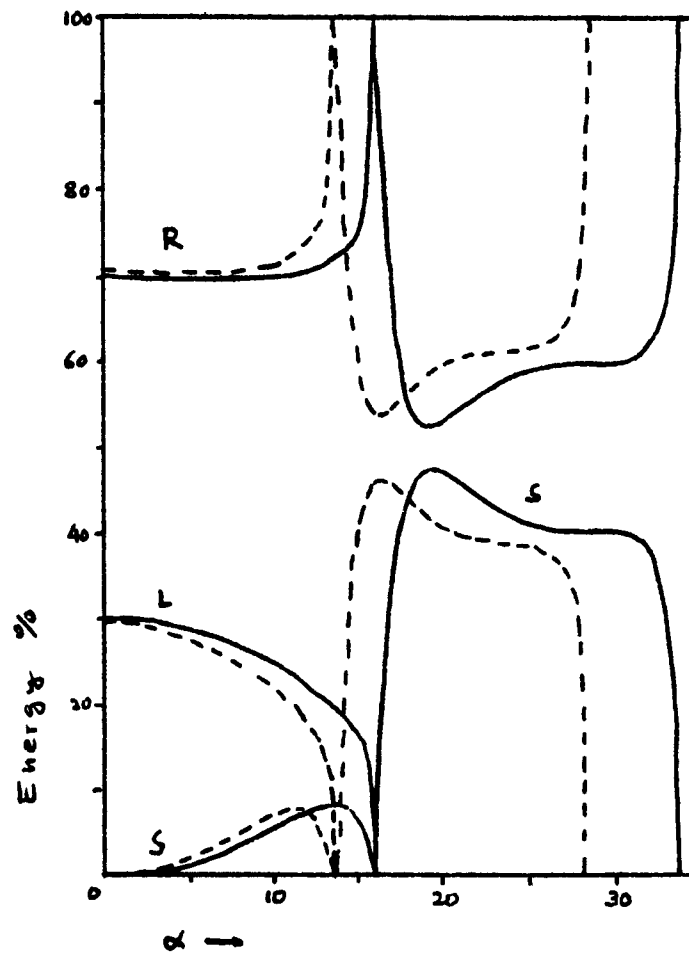


Figure 4. Same as Fig. 1 for aluminum.

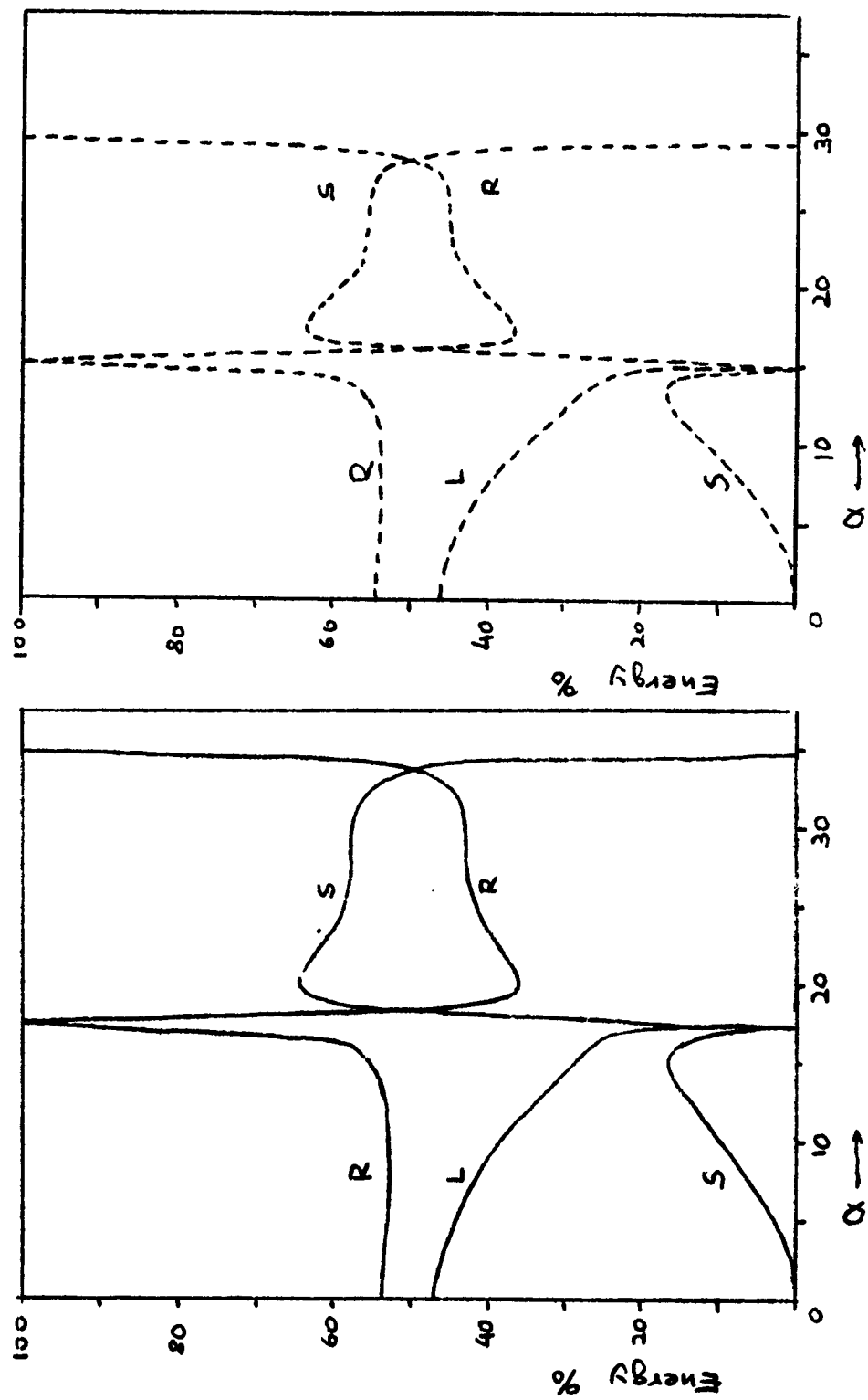


Figure 5. Same as Fig. 1 for magnesium.

LIST OF FIGURES

- Figure 1. Energy relations at oil-steel boundary (solid lines) and water-steel boundary (dashed lines). R reflected wave, L refracted longitudinal wave, S refracted shear wave.
- Figure 2. Same as Fig. 1 for copper.
- Figure 3. Same as Fig. 1 for brass.
- Figure 4. Same as Fig. 1 for aluminum.
- Figure 5. Same as Fig. 1 for magnesium.

BIBLIOGRAPHY

1. D. L. Arenberg, J. Acoust. Soc. Am. 20, 1 (1948).
2. J. Schaefer, Ph.D. Thesis, University of Strassburg (1942).
3. W. G. Mayer and J. F. Kelsey, J. Acoust. Soc. Am. 34, 269 (1962).
4. K. Ergin, Bull. Seism. Soc. Am. 42, 349 (1952).
5. W. J. McGonagle, Nondestructive Testing (McGraw-Hill, New York, 1961).
6. J. Krautkrämer and H. Krautkrämer, Werkstoffprüfung mit Ultraschall (Springer-Verlag, Berlin, Göttingen, Heidelberg, 1961).
7. C. G. Knott, Phil. Mag. 48, 64 (1899).
8. K. Zoeppritz, Mchr. Akad. Wiss. Göttingen, Math-Physik Kl., Ila. Math. physik-chem. Abt. 66 (1919).

DISTRIBUTION LIST FOR UNCLASSIFIED TECHNICAL REPORTS

Office of Naval Research (Code 468)
Department of the Navy
Washington 25, D. C. (2 copies)

Director
U. S. Naval Research Laboratory
Technical Information Division
Washington 25, D. C. (6 copies)

Director
U. S. Naval Research Laboratory
Sound Division
Washington 25, D. C. (1 copy)

Commanding Officer
Office of Naval Research Branch Office
The John Crerar Library Building
86 East Randolph Street
Chicago 1, Illinois (1 copy)

Commanding Officer
Office of Naval Research Branch Office
Box 39, Navy No. 100
FPO, New York (12 copies)

Armed Services Technical Information Agency
Arlington Hall Station
Arlington 12, Virginia (10 copies)

Commander
U. S. Naval Ordnance Laboratory
Acoustics Division
White Oak
Silver Spring, Maryland (1 copy)

Commanding Officer and Director
U. S. Navy Electronics Laboratory
San Diego 52, California (1 copy)

Director
U. S. Navy Underwater Sound Reference
Laboratory
Office of Naval Research
P. O. Box 8337
Orlando, Florida (1 copy)

Western Reserve University
Department of Chemistry
Cleveland, Ohio
(Attn: Dr. E. Yeager) (1 copy)

Commanding Officer and Director
U.S. Navy Underwater Sound Lab.
Fort Trumbull
New London, Connecticut (1 copy)

Commander
U. S. Naval Air Development Center
Johnsville, Pennsylvania (1 copy)

Director
National Bureau of Standards
Connecticut Ave. and Van Ness St., N.W.
Washington 25, D. C.
(Attn: Chief of Sound Section)
(1 copy)

Commanding Officer and Director
David Taylor Model Basin
Washington 7, D. C. (1 copy)

Superintendent
U. S. Navy Postgraduate School
Monterey, California
(Attn: Prof. L.E. Kinsler)(1 copy)

Commanding Officer
U. S. Navy Mine Defense Laboratory
Panama City, Florida (1 copy)

U. S. Naval Academy
Annapolis, Maryland
(Attn: Library) (1 copy)

Harvard University
Acoustics Laboratory
Division of Applied Science
Cambridge 38, Mass. (1 copy)

Brown University
Department of Physics
Providence 12, R. I. (1 copy)

Director
Ordnance Research Laboratory
Pennsylvania State University
University Park, Pa. (1 copy)

Defense Research Laboratory
University of Texas
Austin, Texas

University of California
Department of Physics
Los Angeles, California (1 copy)

University of California
Marine Physical Laboratory
Scripps Institution of Oceanography
San Diego 52, California (1 copy)

Bell Telephone Laboratories
Whippany, N. J. (1 copy)

Director
Columbia University
Hudson Laboratories
145 Palisades Street
Dobbs Ferry, N. Y. (1 copy)

Woods Hole Oceanographic Institute
Woods Hole, Massachusetts (1 copy)

Dr. J. R. Smithson
Electrical Engineering Department
U. S. Naval Academy
Annapolis, Maryland (1 copy)

Edwards Street Laboratory
Yale University
Box 1916 Yale Station
New Haven 11, Conn. (1 copy)

Lamont Geological Observatory
Columbia University
Torrey Cliffs
Palisades, N. Y. (1 copy)

The Catholic University of America
Department of Physics
Washington, D. C. (1 copy)

Massachusetts Institute of Technology
Laboratory of Electronics
Cambridge 39, Mass.
(Attn: Dr. U. Ingard) (1 copy)

Bureau of Naval Weapons
Code RU-222 (Oceanographer)
Washington 25, D. C. (1 copy)

Dr. George Hudson
Department of Physics
New York University
University Heights
New York 53, N. Y. (1 copy)

Bureau of Ships (Code 345)
Department of the Navy
Washington 25, D. C. (1 copy)

Bureau of Ships (Code 688)
Department of the Navy
Washington 25, D. C. (1 copy)

Bureau of Naval Weapons (RUDC)
Department of the Navy
Washington 25, D. C.

U. S. Navy SOFAR Station
APO No. 856, c/o Postmaster
New York, New York
(Attn: Mr. G. R. Hamilton) (1 copy)

John Carroll University
University Heights
Cleveland 18, Ohio
(Attn: E. F. Carome) (1 copy)

Edo Corporation
College Point, L. I., New York
(Attn: C. Loda) (1 copy)

Mr. Fred O. Briggson
ONR Resident Representative
University of Michigan
820 East Washington St.
Ann Arbor, Michigan (1 copy)

Naval Ordnance Test Station
Pasadena 8, California (1 copy)

Applied Physics Laboratory
University of Washington
Seattle, Washington (1 copy)

Dr. W. J. Fry
Biophysical Research Laboratory
University of Illinois
Urbana, Illinois (1 copy)

Institute for Defense Analyses
Communications Research Division
von Neumann Hall
Princeton, New Jersey (1 copy)

Dr. Alfred Weissler
Department of Chemistry
American University
Washington 16, D. C. (1 copy)

Dr. K. L. Zankel
Department of Physics
University of Oregon
Eugene, Oregon (1 copy)